

Gas-Phase Nitrogen Doping of Monolithic TiO₂ Nanoparticle-Based Aerogels for Efficient Visible Light-Driven Photocatalytic H₂ Production

Journal Article

Author(s):

Kwon, Junggou; Choi, Kyoungjun; Schreck, Murielle ; Liu, Tian; Tervoort, Elena; Niederberger, Markus 

Publication date:

2021-11-17

Permanent link:

<https://doi.org/10.3929/ethz-b-000513641>

Rights / license:

[Creative Commons Attribution-NonCommercial-NoDerivatives 4.0 International](#)

Originally published in:

ACS Applied Materials & Interfaces 13(45), <https://doi.org/10.1021/acsami.1c12579>

Funding acknowledgement:

184842 - Nanoparticle-based aerogels for photocatalytic gas phase reactions (SNF)

Gas-Phase Nitrogen Doping of Monolithic TiO₂ Nanoparticle-Based Aerogels for Efficient Visible Light-Driven Photocatalytic H₂ Production

Junggou Kwon, Kyoungjun Choi, Murielle Schreck, Tian Liu, Elena Tervoort, and Markus Niederberger*

Cite This: *ACS Appl. Mater. Interfaces* 2021, 13, 53691–53701

Read Online

ACCESS |

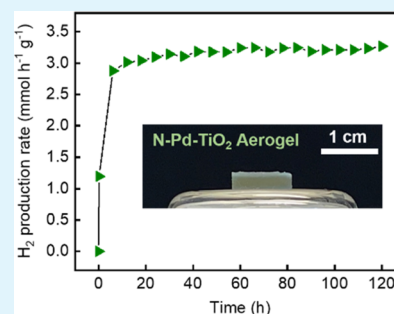
Metrics & More

Article Recommendations

Supporting Information

ABSTRACT: The development of visible light-active photocatalysts is essential for increasing the conversion efficiency of solar energy into hydrogen (H₂). Here, we present a facile method for nitrogen doping of monolithic titanium dioxide (TiO₂) nanoparticle-based aerogels to activate them for visible light. Plasma-enhanced chemical vapor deposition at low temperature enables efficient incorporation of nitrogen into preformed TiO₂ aerogels without compromising their advantageous intrinsic characteristics such as large surface area, extensive porosity, and nanoscale properties of the semiconducting building blocks. By balancing the dopant concentration and the defects, the nitridation improves optical absorption and charge separation efficiency. The nitrogen-doped TiO₂ nanoparticle-based aerogels loaded with palladium (Pd) nanoparticles show a significant enhancement in visible light-driven photocatalytic H₂ production (3.1 mmol h⁻¹ g⁻¹) with excellent stability over 5 days. With this method, we introduce a powerful tool to tune the properties of nanoparticle-based aerogels after synthesis for a specific application, as exemplified by visible light-driven H₂ production.

KEYWORDS: nitrogen-doped titania, aerogels, hydrogen production, photocatalysis, nanoparticles



INTRODUCTION

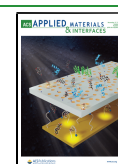
H₂ generation using abundant solar energy together with semiconductor photocatalysts holds significant potential to produce clean and sustainable energy carriers. Among the various photocatalysts for H₂ generation, TiO₂ stands out by its chemical stability, low cost, nontoxicity, and suitable band position with respect to the redox potentials of water splitting.¹ Owing to these attractive features, research has exploited diverse forms of TiO₂ such as powders,² wires,³ rods,⁴ and films⁵ to further enhance its photocatalytic activity. Recently, TiO₂ nanoparticle-based aerogels have emerged as a promising architecture for gas-phase photocatalysis, offering large surface areas, high open porosity, and translucency, which are all advantageous properties for such applications.⁶ TiO₂ aerogels, prepared from colloidal dispersions of nanoparticles obtained by the nonaqueous sol-gel method, fully preserve the intrinsic characteristics of crystalline nanobuilding blocks in macroscopic bodies.⁷ As a new class of three-dimensional photocatalysts,⁸ the nanoparticle-based aerogels have successfully demonstrated their potential for photocatalytic gas-phase reactions such as CO₂ reduction⁹ and H₂ production.¹⁰ However, an intrinsic drawback of TiO₂ is its wide bandgap of 3.2 eV. This limits the working range to ultraviolet (UV), which covers less than ~5% of the solar spectrum. Therefore, different strategies have been explored to modify the electronic structure of TiO₂, including doping with nonmetals^{11,12} and metals^{13–15} to get a visible-light response.

A particularly promising way to engineer TiO₂ is nitrogen doping due to the similar ionic radii of nitrogen and oxygen, demanding less formation energy for substitution. Moreover, the position of the N 2p state above the valence band narrows the bandgap, and the band position remains well aligned with respect to the redox potentials of water splitting.¹⁶ Incorporation of nitrogen has been applied to a wide range of TiO₂ nanostructures to extend the absorption edge to visible light using sputtering,¹⁷ high-temperature annealing (450–650 °C) in an ammonia (NH₃)^{18,19} or N₂ atmosphere,²⁰ and wet chemical methods such as sol-gel^{21,22} and hydrothermal processes.^{23,24} However, activation of TiO₂ aerogels for visible-light utilization by nitrogen doping has not yet been achieved without severely deteriorating the aerogel-specific morphology. For example, immersing TiO₂ aerogels in an aqueous NH₃ solution followed by annealing at 530 °C for 10 min resulted in a low porosity of 0.1 cm³ g⁻¹ and low surface area of 78 m² g⁻¹.²⁵ Another approach to achieve nitrogen doping involved the mixing of TiO₂ aerogel powders with urea solution and

Received: July 4, 2021

Accepted: October 22, 2021

Published: November 3, 2021



subsequent annealing at 550 °C under N₂/NH₃ flow. Also in this case, the surface area of the heat-treated aerogel is relatively low (116 m² g⁻¹).²⁶ Accordingly, the performance of these aerogels for photocatalytic H₂ production in the liquid phase is relatively poor, even when they are combined with platinum nanoparticles as cocatalyst.²⁷ In addition to the morphological features, the concentration of the nitrogen dopant plays an important role in photocatalytic activity because it affects the amount of defects (e.g., oxygen vacancies and Ti³⁺) and, thus, the efficiency of charge separation between the photogenerated electrons and holes.²⁸

Considering the advantages and disadvantages of the different literature reports, the ideal approach to make TiO₂ nanoparticle-based aerogels that are sensitive to visible light must allow nitrogen doping with a precise concentration under full preservation of the aerogel structure. In principle, there are two ways to achieve this. The TiO₂ nanoparticles can already be doped during their synthesis and prior to gelation, or nitrogen doping occurs on the final TiO₂ aerogel. The first method poses the problem of nitrogen-doped TiO₂ nanoparticles being difficult to process into highly stable, concentrated colloidal dispersions as required for the gelation step. The second method has a big advantage such that we do not need to change the synthesis protocol for the aerogels, which is meanwhile optimized and results in high-quality aerogels. The challenge here is to perform the nitrogen doping under experimental conditions that do not affect the fragile structure of the three-dimensional TiO₂ network.

In this study, we present a facile method to postsynthetically dope monolithic and macroscopically large TiO₂ nanoparticle-based aerogels with nitrogen to make them visible light-active for photocatalytic H₂ production. Plasma-enhanced chemical vapor deposition at low temperature using NH₃ gas enables nitrogen doping to improve optical properties while preserving all the favorable characteristics of the preformed aerogels. By a careful evaluation of the synthesis parameters such as temperature and concentration of the NH₃ gas, we optimize the doping process with respect to photoabsorption and charge separation efficiency of the resulting TiO₂ aerogels. Through comprehensive characterizations, we find that the structural and morphological properties, concentration of nitrogen and its position in the lattice, oxygen vacancies, and presence of Ti³⁺ determine photocatalytic activity under visible-light illumination. The best nitrogen-doped Pd-TiO₂ nanoparticle-based aerogels are able to produce ~3.1 mmol h⁻¹ g⁻¹ of H₂ with good stability over 5 days under visible light. Our gas-phase nitridation method offers a powerful tool to modify the chemical composition of nanoparticle-based aerogel monoliths postsynthetically to optimize their properties for a specific application.

EXPERIMENTAL SECTION

Materials. Titanium(IV) tetrachloride (TiCl₄, 99.9% trace metals basis), benzyl alcohol (BnOH, puriss., 99–100.5% (GC)), 2-amino-2-(hydroxymethyl)-1,3-propanediol (Trizma base, puriss., ≥99.7%), palladium(II) acetate ([Pd(OAc)₂]₃, ≥99.9% trace metals basis), and methanol (MeOH, analytical grade) were purchased from Sigma-Aldrich. Acetone (99.8%, extra dry) and chloroform (≥99%, extra pure) were purchased from Acros Organics, and ethanol (absolute, >99.8% for analysis) and diethyl ether (≥99.5%) were purchased from VWR Chemicals. Liquid carbon dioxide (≥99%), argon (Ar, 99.999%), helium (He, 99.999%), nitrogen (N₂, 99.999%), ammonia (NH₃, 99.999%), and argon (Ar, 99.999%) were provided by

PanGas AG, Switzerland. All chemicals were used as received without further purification.

Preparation of TiO₂ and Pd-TiO₂ Nanoparticle-Based Aerogels. TiO₂ and Pd-TiO₂ nanoparticle-based aerogels were prepared by the nonaqueous sol–gel method as reported in the literature.²⁹ First, titanium (IV) tetrachloride (4.5 mL) and 2-amino-2-(hydroxymethyl)-1,3-propanediol (414 mg) were dissolved in 90 mL of benzyl alcohol and stirred at 80 °C for 24 h. The resulting nanoparticles were extracted from the reaction solution by centrifugation and washed three times in chloroform and diethyl ether. The wet nanoparticles were dispersed in deionized water. The residual diethyl ether was removed by applying a vacuum. The concentration of the TiO₂ dispersion was 120 mg/mL. For the synthesis of Pd nanoparticles, palladium (II) acetate (32 mg) in benzyl alcohol (4 mL) was stirred at room temperature for 18 h.³⁰ The synthesized Pd nanoparticles were washed with ethanol three times. After the last centrifugation step, 7.5 mL of ethanol was added to the wet precipitate to get the Pd nanoparticle dispersion. This dispersion was further diluted with ethanol to reach final concentrations of 0.17, 0.33, 0.50, and 0.67 wt %. A 0.3 mL portion of the Pd nanoparticle dispersion was combined with 0.3 mL of TiO₂ dispersion to prepare the sample with Pd. For the sample without Pd, 0.3 mL of ethanol was added to 0.3 mL of TiO₂ dispersion. The gelling was carried out in an oven at 60 °C for 33 min. The solvent was stepwise exchanged against acetone. The samples were immersed into solvent mixtures with different volume ratios in the following order: Acetone/ethanol/water = 70/20/10 (v/v %) for 20 h, 80/15/5 (v/v %) for 6 h, and 100/0/0 (v/v %) for 20 h. The prepared gels were supercritically dried in a SPI-DRY Critical Point Dryer 13200, replacing the acetone with supercritical CO₂. The aerogels were treated with UV light (2000 W) using a Höppler UVACUBE 2000 chamber for 20 h to remove organic residues on the surface.

Process for Nitrogen Doping into Pd-TiO₂ Aerogels.

Nitrogen doping of the Pd-TiO₂ aerogels was carried out by a plasma-enhanced chemical vapor deposition (TCVD-RF100CA, GRAPHENE SQUARE). The aerogel placed in a ceramic crucible boat was put into the chamber, which was heated up to the desired reaction temperature (300–450 °C) for 0.5 h. During the heat-up phase, different amounts of NH₃ gas with a total flow rate of 500 sccm were introduced into the chamber using Ar as carrier gas at a pressure of 1.3 torr. After reaching the temperature, RF plasma (100 W) was applied with continuous heating for 3 h. The Pd-TiO₂ aerogels were treated at different temperatures. Aerogels reacted at 300, 350, 400, or 450 °C under 10% NH₃ are denoted as NPT 300, NPT 350, NPT 400, and NPT 450. In addition, NPT 350 was prepared with various Pd concentrations using colloidal dispersions of 0.17, 0.33, 0.50, and 0.67 wt % labeled as NPT 350-C1, NPT 350-C2, NPT 350-C3, and NPT 350-C4, respectively. Samples treated with different NH₃ concentrations (5, 10, 15, or 20%) at 350 °C and with 0.50 wt % Pd are named as NPT 350-5, NPT 350-10, NPT 350-15, and NPT 350-20, respectively. The TiO₂ aerogel treated at 350 °C under 10% NH₃ is named as N-TiO₂, and the Pd-TiO₂ aerogel treated under Ar (500 sccm) at 350 °C is labeled as Ar-Pd-TiO₂ 350. Table S1 provides an overview of all the samples with their names, temperatures of NH₃ treatment, and NH₃ and Pd concentrations.

Characterization. Powder X-ray diffraction (XRD) patterns were recorded on a PANalytical Empyrean with a PIXcel ID detector and Cu K_α radiation. Ultra-high resolution scanning electron microscopy (Hitachi SU8200) was conducted at 2 μA and 1 kV. High-resolution transmission electron microscopy (HRTEM) images were taken with a FEI Talos F200X microscope operated at 200 kV. Nitrogen gas sorption was performed on a Quantachrome Autosorb iQ analyzer at 77 K. The surface area was measured by Brunauer–Emmett–Teller (BET) method, and the pore size and volume were determined by density functional theory (DFT) analysis using a nonlocal DFT (NLDF) calculation model for nitrogen at 77 K based on cylindrical pores in silica. UV–visible spectra were obtained using a JASCO V-770 spectrophotometer equipped with an ILN-725 integrating sphere. X-ray photoelectron spectra (XPS) were recorded by a Sigma 2 spectrometer (Thermo Scientific) using a polychromatic Al K_α X-ray

source by taking C 1s = 284.8 eV as the calibration peak. The atomic concentration was calculated from the individual peak area of Ti, O, and N and their respective atomic sensitivity factor. Electrochemical measurements were conducted with Biologic VMP3 in a three-electrode cell configuration consisting of a platinum wire as the counter electrode and Ag/AgCl as the reference electrode. The aerogel (5 mg) was powdered, dispersed in ethanol (1 mL), and spin-coated on FTO glass as the working electrode. Aqueous Na₂SO₄ solution (0.5 M) was used as the electrolyte and an LED (Thorlabs, nominal wavelength: 450 nm, wavelength range: 400–500 nm) irradiated the system during measurement. The transient photocurrent responses vs time were monitored at a bias potential of +0.2 V with ON/OFF irradiation cycles. With the same system, Nyquist plots were recorded by electrochemical impedance spectroscopy (EIS) in the frequency range of 0.1–100 kHz with an ac amplitude of 5 mV under an open circuit.

Photocatalytic H₂ Production Test. Photocatalytic H₂ production was conducted in gas phase under visible-light irradiation at room temperature. The aerogel was placed inside a homemade reactor, and two LEDs (Thorlabs, nominal wavelength: 450 nm, wavelength range: 400–500 nm) were mounted on both sides of the reactor to measure TiO₂, Pd-TiO₂, and all NPT aerogels (Figure S1). NPT 350-10 was additionally measured with a broader range of wavelengths using two Thorlabs White LEDs (wavelength range: 400–800 nm). The vapor of water and methanol (50:50 v/v) was delivered to the aerogel by Ar as a carrier gas with a flow rate of 10 mL min⁻¹. A gas chromatograph (Inficon Micro-GC 3000A, equipped with He and Ar carrier gas) analyzed the H₂ production with a thermal conductivity detector, and the rate with the corresponding standard deviation was determined by the amount obtained at 3 h using three different samples with the same composition. The apparent quantum efficiency (AQE) was calculated according to the following equation³¹

$$\begin{aligned} \text{QE}(\%) &= \frac{\text{number of reacted electrons}}{\text{number of incident photons}} \times 100 \\ &= \frac{2 \times \text{number of evolved H}_2 \text{ molecules}}{\text{number of incident photons}} \times 100 \end{aligned}$$

The details of AQE (%) calculations are explained in the Supporting Information (Figure S2).

RESULTS AND DISCUSSION

The process of doping preformed TiO₂ nanoparticle-based aerogel monoliths with nitrogen is illustrated in Figure 1a. We employed a plasma-enhanced chemical vapor deposition process to decompose NH₃ into active species such as NH_x,

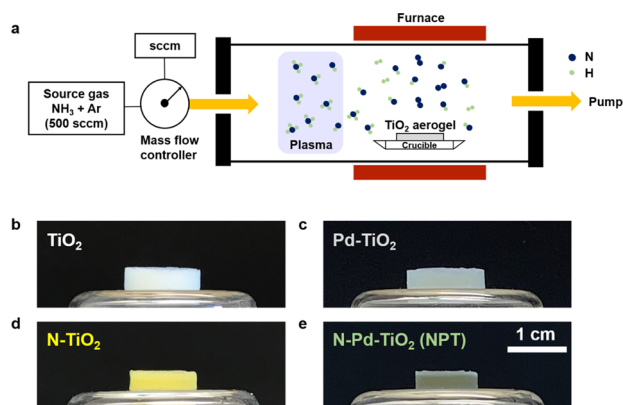


Figure 1. (a) Schematic illustration of the nitridation process of a monolithic TiO₂ nanoparticle-based aerogel by plasma-enhanced chemical vapor deposition. Digital photographs of aerogel monoliths composed of (b) TiO₂, (c) Pd-TiO₂, (d) N-TiO₂, and (e) N-Pd-TiO₂ (NPT 350).

N₂, and H₂ at specific temperatures in the range of 300–450 °C. As shown in Figure 1b–e, a color change from white and light gray to yellow and dark green, respectively, is observed in the TiO₂ and Pd-TiO₂ aerogels after nitridation, indicating the modification of the optical properties and, thus, successful incorporation of nitrogen into the TiO₂ lattice. The highly porous structure of the aerogel facilitates the homogeneous diffusion of dissociated NH₃ molecules throughout the entire monolith. In addition, the large surface area enhances the rate of the doping reaction by offering more active sites.

The crystal structures of Pd-TiO₂ and nitrogen-doped Pd-TiO₂ aerogels (NPT) prepared at 300, 350, 400, and 450 °C (labeled as NPT 300, NPT 350, NPT 400, and NPT 450) were characterized by X-ray powder diffraction (XRD) (Figure 2a). The XRD pattern of Pd-TiO₂ can be assigned to the anatase phase (ICDD file card no. 1-70-6826). The high crystallinity of the pristine Pd-TiO₂ without any high-temperature annealing is one of the advantages of nanoparticle-based aerogels prepared from nanocrystalline building blocks. The sharp peak at (004) is a consequence of the oriented attachment of Trizma-functionalized TiO₂ nanoparticles during gelation.³² After nitridation, the crystal structure remains unchanged as anatase, and peaks that could be attributed to the presence of TiN are not observed. The main differences in the XRD patterns before and after nitridation are the more distinct peaks with reduced full width at half maximum (FWHM), indicating improved crystallinity and some crystal growth. Indeed, as shown in Table S2, this observation is confirmed by calculating the crystal size from the (101), (004), and (200) peaks by the Scherrer equation. The crystallite sizes of Pd-TiO₂, NPT 300, NPT 350, NPT 400, and NPT 450 are 3.9, 4.6, 5.6, 6.5, and 7.5 nm, respectively.

Scanning electron microscopy (SEM) and high-resolution transmission electron microscopy (HRTEM) were performed to explore the morphology of the aerogel after nitridation at 350 °C (NPT 350). In Figure 2b, the SEM image shows a continuous and percolating network of the nanoparticles, indicating that the nitridation treatment preserves the high open porosity of the aerogel (Figure S3). The HRTEM image in Figure 2c presents the lattice spacing of 0.24 nm for the (004) plane and 0.35 nm for the (101) plane of the anatase phase, which is consistent with the XRD result. As we reported before, the connection of the TiO₂ nanoparticles is based on oriented attachment along [001] as a result of the selective desorption of Trizma from the (001) facets in aqueous solution.³³ The HRTEM image in Figure 2d shows that the nitrogen-doped TiO₂ nanoparticles are indeed, at least in part, arranged crystallographically along [001], consistent with the structure discussed in pure TiO₂ aerogels.³² This behavior was expected, of course, as we start with Trizma-functionalized TiO₂, and the nitrogen doping is performed after the gelation and drying step. In fact, the SEM and TEM results clearly underline that the gas-phase nitridation does not influence the structure and arrangement of the TiO₂ nanoparticles in the aerogel. N₂ gas sorption analysis was performed to investigate the pore size distribution, porosity, and surface area of Pd-TiO₂, NPT 300, NPT 350, NPT 400, and NPT 450. The adsorption–desorption isotherms of Pd-TiO₂, NPT 300, NPT 350, and NPT 400 are of type IV with hysteresis loops of combined H1 and H3, which is characteristic for mesopores (Figure 2e). The absence of a plateau in the high-relative pressure region indicates the presence of macropores in the

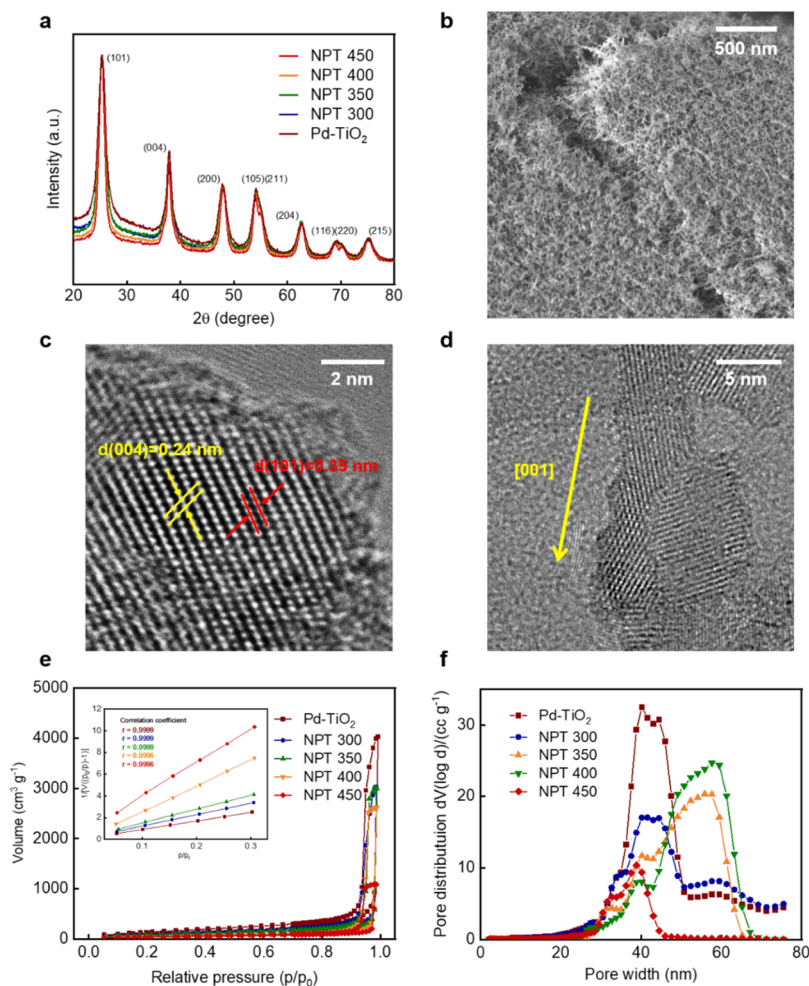


Figure 2. (a) Powder XRD patterns of Pd-TiO₂, NPT 300, NPT 350, NPT 400, and NPT 450. (b) SEM image and (c, d) HRTEM images of NPT 350. (e) N₂ adsorption–desorption isotherms (inset, corresponding BET isotherms) and (f) DFT pore size distribution of Pd-TiO₂, NPT 300, NPT 350, NPT 400, and NPT 450.

aerogels, which is also confirmed by the density functional theory (DFT) analysis of the pore size distributions in Figure 2f. Compared to Pd-TiO₂, NPT 350 and NPT 400 show a shift to a broader pore size distribution and to larger pores from 40 to 60 nm due to the partial sintering of the nanoparticles. For NPT 450, the disappearance of the macropores is consistent with the isotherm of H1 hysteresis loop, displaying only mesopores due to volume contraction of the aerogel after such a high-temperature treatment.³⁴ As presented in Table S2, NPT 300 and NPT 350 offer relatively high surface areas (325.1 and 267.8 m² g⁻¹) with large pore volumes (4.1 and 4.4 cm³ g⁻¹), which are beneficial for photocatalytic reactions. Although NPT 400 and NPT 450 have considerably reduced values of the surface area (144.7 and 109.2 m² g⁻¹) with small pore volumes (3.9 and 1.3 cm³ g⁻¹), the integrity of the monolithic bodies remains intact with a porous structure even after nitridation at 450 °C (Figure S4). The results demonstrate that the porosity and surface area typical for aerogels vary depending on the temperatures but can be fully preserved in the low-temperature-treated samples (NPT 300 and NPT 350).

To evaluate the chemical composition and nitrogen concentration, Pd-TiO₂, NPT 300, NPT 350, NPT 400, and NPT 450 were carefully analyzed by X-ray photoelectron spectroscopy (XPS). First, the N 1s spectra were deconvoluted

into four regions as shown in Figure 3a. The peak positioned at 396.1 eV is known as substitutional doping (Ti-N). It proves the replacement of oxygen by nitrogen in the TiO₂ lattice, narrowing the bandgap by forming N 2p states mixed with O 2p above the valence band.^{16,18} The peak around 400.5 eV agrees well with XPS data of interstitial doping in the form of Ti-O-N, which also generates a new energy N 2p level above the valence band.^{35–37} The peak at 399.9 eV is attributed to NH₂ species from Trizma on the surface of the aerogel.³³ The last peak at the highest binding energy (402 eV) can be assigned to molecular N₂.^{38,39} These last two peaks were also detected in the pristine sample (Figure S5). It appears that the substitutional doping of N starts to occur at 350 °C, which is a relatively low temperature compared to other NH₃ annealing methods.^{3,40,41} From a concentration point of view, it seems that higher temperatures do not allow for higher nitrogen doping. However, with increasing temperature, the proportion of substitutional doping relative to interstitial doping increases from 0% (NPT 300) to 0.05% (NPT 350), 0.07% (NPT 400), and finally 0.15% (NPT 450) (Figure 3b), suggesting that higher temperatures are necessary to obtain substitutional doping. It is known that nitrogen doping lowers the formation energy of oxygen vacancies and facilitates the reduction of Ti⁴⁺ to Ti³⁺ in TiO₂.^{42,43} The result of XPS Ti 2p in Figure 3c supports that substitutional and interstitial defects are both

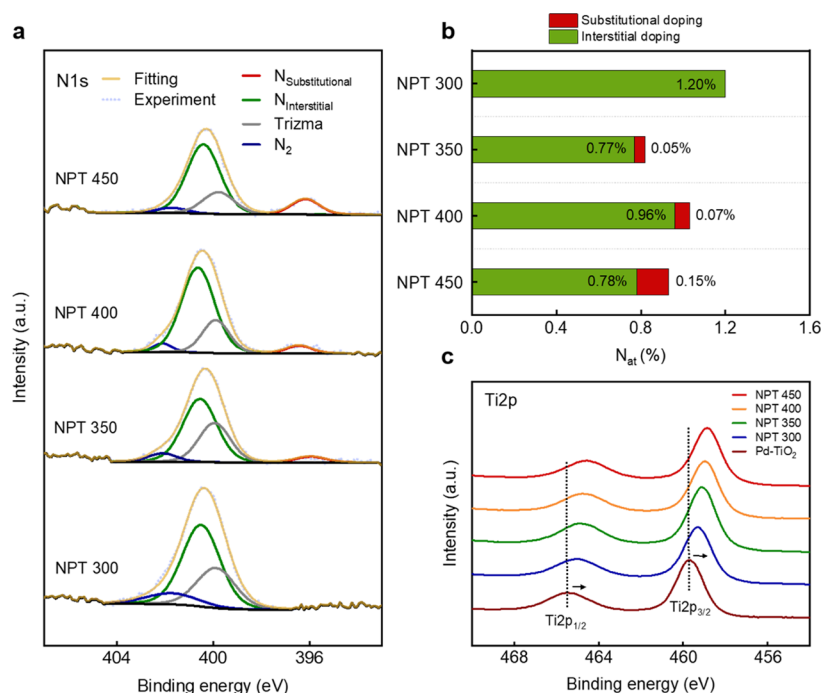


Figure 3. (a) XPS N 1s spectra and (b) atomic percentage of nitrogen doping (substitutional and interstitial) in NPT 300, NPT 350, NPT 400, and NPT 450. (c) XPS Ti 2p spectra of Pd-TiO₂, NPT 300, NPT 350, NPT 400, and NPT 450.

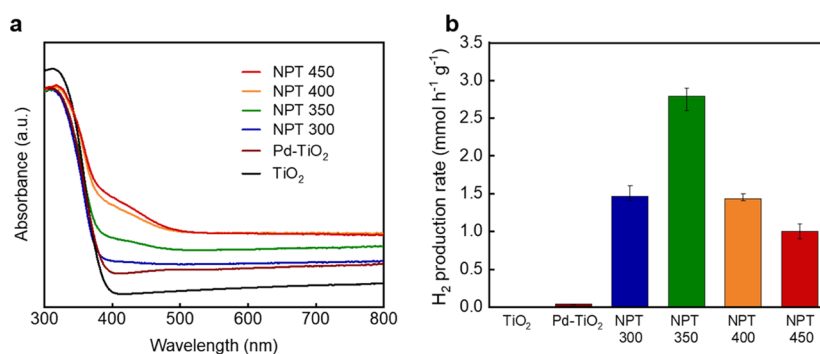


Figure 4. (a) UV-Vis diffuse reflectance spectra and (b) visible light-driven photocatalytic H₂ production rate of TiO₂, Pd-TiO₂, NPT 300, NPT 350, NPT 400, and NPT 450.

concurrent in the NPT samples. Compared to Pd-TiO₂, the peak of Ti⁴⁺ of the NPT samples shifted to lower binding energies, indicating the presence of Ti³⁺ in TiO₂.⁴⁴ Moreover, the atomic percentage of Ti³⁺ increased from 5.8 to 11.4% with increasing temperature, and the reason for this result is that the nitridation using NH₃ gas in Ar at higher temperature releases more H₂, which can partially reduce TiO₂ (Figure S6).¹⁹ Investigation of the chemical state of the Pd nanoparticles before (Pd-TiO₂) and after nitridation (NPT 350) showed in the XPS-Pd 3d spectra that the Pd nanoparticles in both aerogels were partially oxidized, but NPT 350 contained more Pd(0) than Pd-TiO₂ due to the effect of the reducing environment (Figure S7).

The optical properties are important for investigating the effect of nitrogen doping, and therefore, UV-visible absorption of TiO₂, Pd-TiO₂, NPT 300, NPT 350, NPT 400, and NPT 450 aerogels were studied. Figure 4a indicates that the band edge of TiO₂ and Pd-TiO₂ ends approximately at 400 nm without any visible-light absorption, whereas the NPT samples exhibit noticeable absorption in the visible region.

According to previous literature, the range of 400–500 nm represents the N 2p states in the bandgap⁴⁵ and the broad absorption in the region of 400–800 nm derives from oxygen vacancies and Ti³⁺, which are formed below the conduction band.^{46,47} In contrast to NPT 350, NPT 400 and NPT 450 respond to visible light more efficiently, implying that a high concentration of nitrogen doping and defects are important for visible-light sensitivity. Although NPT 300 has the highest amount of nitrogen doping (Figure 3b), it shows the lowest visible-light absorption among the NPT aerogels. This observation suggests that the substitutionally doped nitrogen in TiO₂ influences the visible-light response more dominantly compared to the interstitial doping. It can be inferred that the improved optical property is the consequence of excitation from the N 2p state to the conduction band as well as from both the N 2p state and valence band to the impurity level in the electronic structure.

The average photocatalytic H₂ production of TiO₂, Pd-TiO₂, NPT 300, NPT 350, NPT 400, and NPT 450 was evaluated in the gas phase under visible light (Figure 4b). The monolithic

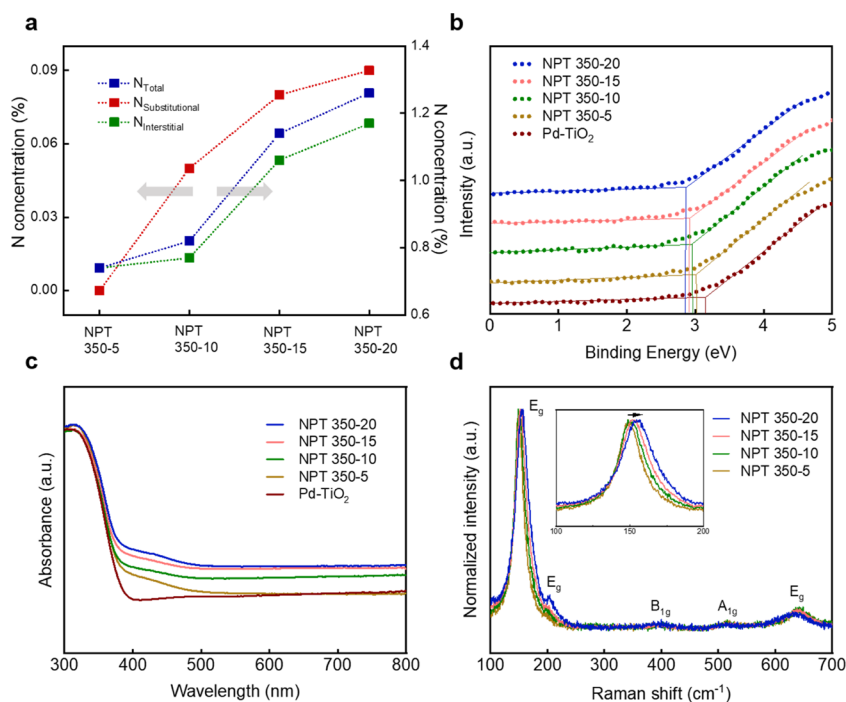


Figure 5. (a) Nitrogen concentration in at % in NPT 350-5, NPT 350-10, NPT 350-15, and NPT 350-20 according to substitutional (red), interstitial (green), and total doping (blue). (b) XPS valence band spectra and (c) UV-Vis diffusion reflectance spectra of Pd-TiO₂, NPT 350-5, NPT 350-10, NPT 350-15, and NPT 350-20. (d) Raman spectra of NPT 350-5, NPT 350-10, NPT 350-15, and NPT 350-20 (inset: magnified E_g peak).

aerogel placed in a sample holder was inserted in a custom-built continuous gas flow reactor (Figure S1). The design of the holder made it possible to orient the aerogel pellet perpendicular to two Thorlabs LEDs to ensure illumination of the entire area. Ar gas (10 mL min⁻¹) was bubbled through a water–MeOH mixture (1:1 v/v) and guided to the aerogel. When using monolithic aerogels as macroscopic photocatalysts, it is important that the reactants are in the gas phase. Contact with liquids would lead to pulverization of the monoliths due to strong capillary forces. The H₂ production was then measured by a gas chromatograph. TiO₂ alone did not produce any H₂ gas at all due to its lack of visible-light sensitivity and fast recombination between the photogenerated electrons and holes. In comparison, N-TiO₂ showed some but very low H₂ production rate of 0.05 mmol h⁻¹ g⁻¹ because of enhanced visible-light absorption that allows some charge generation (Figure S8a,b). Pd-TiO₂ produced 0.04 mmol h⁻¹ g⁻¹, which is much better than pure TiO₂ but comparable to N-TiO₂. This observation confirms that Pd nanoparticles in combination with TiO₂ improve the charge separation by acting as electron sinks,¹⁰ but the effect is not greater than the improvement of visible-light absorption properties by nitrogen doping. The H₂ evolution rates of NPT 300, NPT 350, NPT 400, and NPT 450 were remarkably enhanced, and NPT 350 especially showed a high rate of 2.8 mmol h⁻¹ g⁻¹, which is 70 times higher than that of undoped Pd-TiO₂. The enhanced photocatalytic activity of NPT aerogels compared to Pd-TiO₂ is probably a result of the significant increase in visible-light absorption, which offers photogenerated electrons for the reduction of H⁺ to H₂. Moreover, the localized states below the conduction band induced by Ti³⁺ and oxygen vacancies are known to function as electron acceptors, increasing the driving force for charge separation and enhancing the performance.^{48,49} In addition to the effect of nitrogen doping on

photocatalytic activity, there are two other factors that must be considered. The higher fraction of the metallic state of Pd after nitridation resulted in a better charge transport, which can also contribute to higher efficiency. The degree of crystallinity of the semiconductor nanoparticles in the aerogel is expected to influence the yield as well, and this possibility is supported by the enhanced H₂ production rate of Pd-TiO₂ annealed under Ar environment at 350 °C (Ar-Pd-TiO₂ 350) (Figure S8b). A comparison of the XRD patterns of Pd-TiO₂ and Ar-Pd-TiO₂ 350 (Figure S8c) indeed shows a higher intensity of the reflections for Ar-Pd-TiO₂ 350, and the crystallite sizes calculated with the Scherrer equation from the (101), (004), and (200) peaks are also larger for Ar-Pd-TiO₂ 350 (5.5 nm) with respect to 3.5 nm found for Pd-TiO₂. Compared to the best performance of NPT 350, NPT 300 produced only 1.5 mmol h⁻¹ g⁻¹, suggesting that efficient absorption of visible light is critical for a high H₂ production rate. However, the values of NPT 400 and NPT 450 were lower, namely 1.4 and 1.0 mmol h⁻¹ g⁻¹, respectively, despite the higher visible-light absorption compared to NPT 350. The results imply that the excessive nitrogen doping lowers the photocatalytic efficiency due to an increase in oxygen vacancies again by acting as recombination centers for the photogenerated charge carriers.^{19,28} Moreover, we have to consider that aerogels treated at 400 °C and higher have reduced surface area and lower porosity, which are expected to negatively affect photocatalytic activity due to fewer active sites for H₂ production.

When using TiO₂ in photocatalysis, the concentration of the cocatalyst plays a vital role in elongating the lifetime of photogenerated electrons and holes.⁹ In this study, we varied the concentrations of the Pd nanoparticles as cocatalyst in the TiO₂ aerogels from 0.17, 0.33, and 0.50 to 0.67 wt %, and we explored the concentration effect on photocatalytic activity after nitrogen doping at 350 °C. As displayed in Figure S9a,

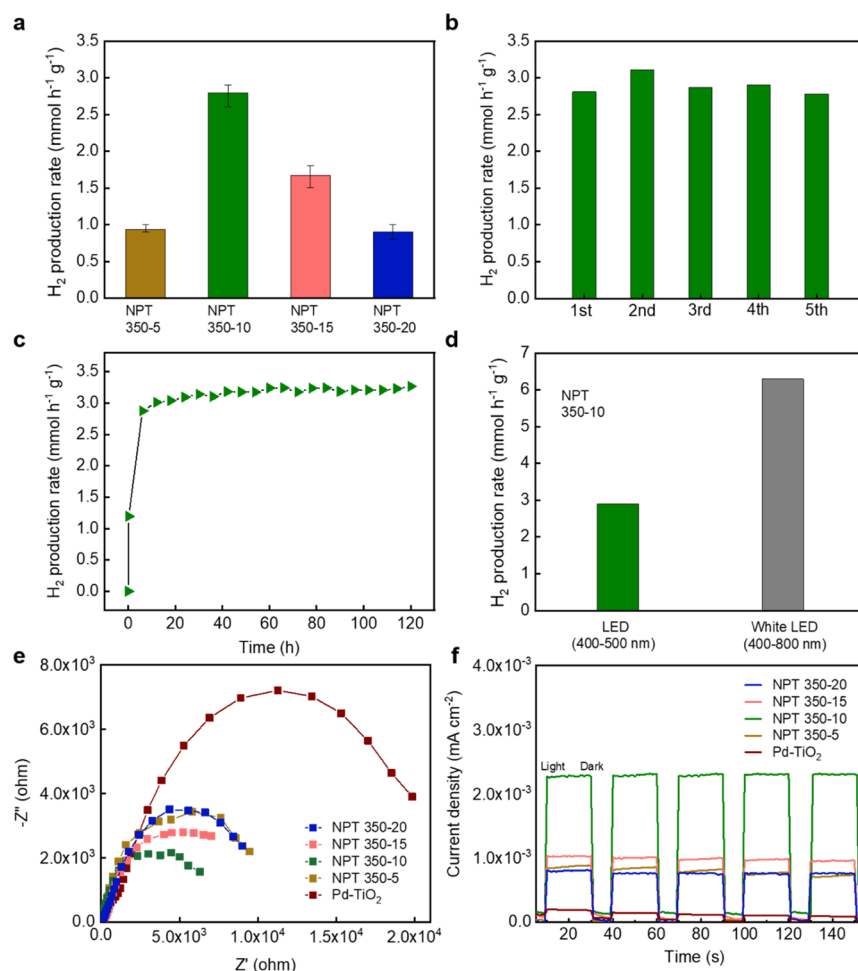


Figure 6. (a) Visible light-driven photocatalytic H₂ production rate of NPT 350-5, NPT 350-10, NPT 350-15, and NPT 350-20. (b) Repeatability and (c) stability test of NPT 350-10. (d) H₂ production rate of NPT 350-10 using LEDs (wavelength: 400–500 nm) and white LEDs (wavelength: 400–800 nm). (e) EIS Nyquist plots and (f) transient photocurrent density–time curves of Pd-TiO₂ and NPT 350-5, NPT 350-10, NPT 350-15, and NPT 350-20.

the average H₂ production rate shows a pronounced dependence on the concentration of the Pd nanoparticles. From 0.17 to 0.50 wt %, the H₂ production rate increases until it reaches a maximum at 0.50 wt %, and then it drops again for a concentration of 0.67 wt %. XPS N 1s spectra indicate that the fraction of substitutional doping increases from 0.01 to 0.11% with increasing Pd nanoparticle concentration from 0.17 to 0.67 wt % (Figure S9b), while the interstitial doping remains basically constant for all samples. The observation that more substitutional doping is induced in the lattice with increasing amount of Pd nanoparticles can be explained by the fact that Pd nanoparticles act as a catalyst, facilitating adsorption and decomposition of NH₃ molecules.⁵⁰ As discussed before, there is an optimum concentration of doping and defects. If this value is exceeded like in NPT 350-C4 (0.67 wt %), the photocatalytic performance for H₂ production drops. The 0.50 wt % was identified as the ideal concentration of Pd nanoparticles in TiO₂ aerogels for effective photocatalytic H₂ production under visible light.

To investigate the influence of the nitrogen concentration in the TiO₂ nanoparticles on their photocatalytic activity, different amounts of NH₃ were introduced into the chamber at a constant temperature of 350 °C. Depending on the NH₃ concentration (5, 10, 15, and 20%), the samples are labeled as

NPT 350-5, NPT 350-10, NPT 350-15, and NPT 350-20. First, XPS analysis was used to explore the change in the nitrogen concentrations and in the chemical composition of the samples. The N 1s spectra were deconvoluted (Figure S10) and the amount of substitutional and interstitial nitrogen is plotted in Figure 5a. There is a clear trend that higher NH₃ gas concentrations also lead to higher dopant concentrations at substitutional and interstitial sites. The result suggests that 5% of NH₃ gas is not enough to induce substitutional doping. In contrast, NPT 350-10, NPT 350-15, and NPT 350-20 have a fraction of substitutional doping, i.e., they have nitrogen that is located at the oxygen sites with concentrations increasing from 0.05 to 0.09%. The dependence of dopant concentration and type of defects on the amount of NH₃ in the chamber offers a simple tool to tune the properties of the Pd-TiO₂ aerogels.⁵¹ The study of the valence band edge by XPS provides valuable information on the change of the electronic structure in TiO₂ after doping with nitrogen (Figure 5b). The difference between the valence band maximum and Fermi-level energy revealed a shift toward the Fermi level of 0 eV from Pd-TiO₂ to NPT 350-20. It seems that a higher dopant concentration leads to a higher density of nitrogen states formed by substitutional and interstitial doping above the valence band, generating a narrower bandgap.⁵² The modified bandgap of the NPT

samples can account for the UV–Vis spectroscopy results, as more nitrogen energy levels generated in Pd-TiO₂ allow for better absorption of visible light. As presented in Figure 5c, NPT 350-20 absorbs visible light the most compared to the other samples, which is due to its heavily doped state.

Raman measurements were carried out to monitor any structural changes of NPT 350-5, NPT 350-10, NPT 350-15, and NPT 350-20 (Figure 5d). The spectra are typical for the anatase phase of TiO₂ with the strongest band (E_g) around 148 cm⁻¹.⁵³ The inset of Figure 5d shows a noticeable shift and broadening of the E_g peak with increasing NH₃ content from 5 to 20%. This observation is an indication for the degree of structural disorder such as oxygen vacancies and Ti³⁺ in the NPT aerogels.⁵⁴ Obviously, a higher NH₃ gas concentration to induce a higher nitrogen doping level also resulted in a higher number of defects in the aerogels. The result agrees well with the XPS Ti 2p spectra of the samples, which exhibited the peak shift to the lower binding energies with increasing the nitrogen concentration due to the higher amount of Ti³⁺ (Figure S11).

The average H₂ production rate under visible-light irradiation was investigated to evaluate the effect of NH₃ gas concentrations on the photocatalytic activity of NPT 350-5, NPT 350-10, NPT 350-15, and NPT 350-20 (Figure 6a). The samples showed significantly different H₂ production rates, which can be attributed to differences in photoabsorption and photogenerated charge separation, which in turn depend on the concentration of nitrogen doping and the nature of the defects. As explained before, the visible-light sensitivity of nitrogen-doped TiO₂ strongly influences photocatalytic activity, because the electrons for the reduction process result from excitation from the N 2p states. Therefore, the relatively low H₂ production rate of 0.9 mmol h⁻¹ g⁻¹ for NPT 350-5 is mainly due to its insufficient visible-light absorption. At the same time, the strong visible-light absorption of highly doped NPT 350-15 and NPT 350-20 did not necessarily assure a high photocatalytic activity, probably due to the rapid recombination of the photogenerated charges at abundant defect sites.²⁸ Obviously, the optimal nitrogen doping together with the appropriate type of defects have to make sure that not only the visible-light absorption is enhanced but also that charge separation is facilitated to get a high photocatalytic performance. In our case, the best-performing sample is NPT 350-10, which showed a H₂ production rate of 2.8 mmol h⁻¹ g⁻¹ under visible-light illumination. Unfortunately, it is difficult to provide a reasonable comparison of our H₂ production rate with the values reported in the literature, because completely different measurement setups (e.g., light irradiation source, reactor type, and sacrificial agent) were used for the photocatalytic reactions. However, when we look at the literature data where photocatalytic H₂ production was recorded under comparable conditions (i.e., nitrogen-doped TiO₂, metal cocatalysts, use of a mixture of water and methanol, room temperature, and illumination with UV–visible light), our H₂ production rate is among the best reported to date, especially considering that we used only visible light for the reaction.^{21,55–57}

To investigate the possibility to reuse the aerogels for H₂ production, a cycling test with NPT 350-10 was carried out five times under the same conditions (i.e., after 3 h of H₂ production, the reactor was purged with Ar gas without illumination for 3 h, and then the photocatalytic tests were repeated). The H₂ production rates were 2.8, 3.1, 2.9, 2.9, and 2.8 mmol h⁻¹ g⁻¹, respectively (Figure 6b), indicating that the

monolith can indeed be recycled several times without losing photocatalytic activity. For the long-term stability, H₂ generation of NPT 350-10 was demonstrated over 5 days with an average rate of 3.1 mmol h⁻¹ g⁻¹ (Figure 6c). As discussed earlier, NPT 350-10 can absorb visible light in the range between 400 and 800 nm. To prove its photocatalytic activity at a wavelength larger than 500 nm, white LEDs (wavelength range: 400–800 nm) were used. The H₂ production rate showed 6.3 mmol h⁻¹ g⁻¹ under these conditions, confirming that NPT 350-10 is indeed visible light-active (Figure 6d).

The apparent quantum efficiency (AQE) was measured under the same condition like the photocatalytic H₂ production using LEDs with the nominal wavelength of 450 nm. For the number of evolved H₂ molecules, the H₂ rate (mol s⁻¹) was used. The amount of photon energy was calculated from the energy of 1 mol of photons, the light intensity on the aerogel, and the irradiation area, which is the aerogel size. The calculated AQE of H₂ production in NPT 350-10 is 5.6%.

Photoelectrochemical measurements were conducted to examine the photogenerated charge transfer efficiency and verify the mechanism of the enhanced photocatalytic activity under visible light. First, Nyquist plots of Pd-TiO₂, NPT 350-5, NPT 350-10, NPT 350-15, and NPT 350-20 were obtained by electrochemical impedance spectroscopy (EIS) (Figure 6e). Obviously, Pd-TiO₂ has the largest semicircle, which is related to the low charge generation due to the limited optical absorption. In contrast, NPT 350-10 exhibits the smallest semicircle diameter among all samples, proving its high conductivity or, in other words, its ability to effectively separate the photogenerated electrons and holes. NPT 350-15 and NPT 350-20 show a higher charge transfer resistance, suggesting an increased recombination rate of charge carriers induced by the large amount of Ti³⁺ and oxygen vacancies.^{18,19} The larger semicircle of the least-doped NPT 350-5 indicates a low conductivity due to the insufficient response to visible light. For further measurements, the transient photocurrent responses were determined by turning the visible-light irradiation on and off (Figure 6f). As expected, unlike the NPT aerogels, Pd-TiO₂ shows almost no changes in photocurrent density with and without illumination. NPT 350-5, NPT 350-15, and NPT 350-20 exhibit some photocurrent response, which, however, is significantly smaller than that of NPT 350-10. NPT 350-10 clearly shows the highest current density of 2.3 × 10⁻³ mA cm⁻² and, thus, the highest response to visible light. This result confirms once again that nitrogen doping in this sample is ideal for promoting visible-light induced charge generation and separation, leading to the best photocatalytic activity under visible-light illumination among all the studied aerogels.

Monolithic aerogels composed of nitrogen-doped Pd-TiO₂ nanoparticles offer several features that contribute to high photocatalytic efficiency for H₂ generation on the level of the individual building blocks as well as on the level of the macroscopic body. Under optimized synthesis conditions, not only the concentration of nitrogen as dopant can be controlled in the TiO₂ lattice but also the type of defect can be tuned. The amount of Pd can be defined during the preparation of the colloidal nanoparticle dispersion, and the chemical state of Pd, which influences charge separation, is affected by the experimental conditions used for the nitridation process. The monolithic aerogel provides a high surface area and high open porosity, both of which yield a high number of reactive sites

and good interaction between gas and photocatalyst. Taking all these considerations together, we propose the following mechanism for the photocatalytic H₂ production under visible light using nitrogen-doped Pd-TiO₂ nanoparticle-based aerogels (Figure 7). Based on XPS analysis, the relatively high

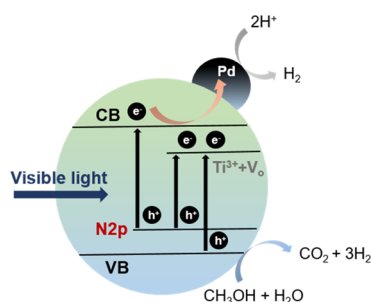


Figure 7. Schematic representation of the photoexcitation process in a nitrogen-doped TiO₂ nanoparticle with Pd as cocatalyst under visible light, leading to the formation of H₂ and oxidation of methanol.

temperature and the concentration of NH₃ gas facilitate the doping of nitrogen into TiO₂. The formation of N 2p states and the narrowing of the bandgap improve the visible-light response. Furthermore, the presence of oxygen vacancies and the resulting Ti³⁺ below the conduction band induced by the nitriding atmosphere act as color centers and electron traps. Therefore, the excitation of electrons from the N 2p state to the conduction band and the excitations of electrons from both N 2p and O 2p states to the localized states formed by defects are responsible for the high efficiency of this process under visible light. With the help of the Pd nanoparticles as cocatalysts loaded on the surface of the nitrogen-doped TiO₂ network, the migration of the photogenerated electrons can be facilitated to promote H₂ production. The photogenerated holes participate in the oxidation of CH₃OH, producing H₂. However, characterization of the samples by Raman, X-ray photoelectron, and impedance spectroscopy indicated that beyond a certain level of nitrogen doping, undesirable oxygen vacancies and Ti³⁺ are generated that act as recombination centers.

CONCLUSIONS

We demonstrated that aerogel monoliths built up by nitrogen-doped Pd-TiO₂ nanoparticles are powerful, three-dimensional photocatalysts for the production of H₂ from methanol and water under visible-light illumination. The preformed aerogels can be doped with nitrogen in a simple gas-phase nitridation process using plasma-enhanced chemical vapor deposition, which makes them sensitive to visible light. Most importantly, this process fully preserves the monolithic structure of the aerogels as well as their material-specific advantages including the large surface area, the pronounced open porosity and the nanoscale features of the building blocks. We demonstrated that the reaction temperature and amount of NH₃ during nitridation strongly influenced the chemical states and nitrogen doping concentration at substitutional and interstitial sites, allowing us to achieve a narrower band gap as well as control over the defect chemistry. In spite of the low nitridation temperature, the crystallinity of the aerogels is slightly improved, which has an additional positive effect on photocatalytic activity. Along with the ideal loading and the chemical state of Pd nanoparticles, the most active sample showed

remarkably enhanced visible light-driven photocatalytic H₂ production up to 3.1 mmol h⁻¹ g⁻¹ (70 times higher than undoped Pd-TiO₂ aerogel) with excellent long-term stability. The greatly improved photocatalytic performance is a result of the optimized doping conditions, which provide an appropriate trade-off between photoabsorption and charge separation efficiency. Our gas-phase nitriding process for modifying preformed aerogel monoliths enables systematic improvement of the photocatalytic efficiency of nanoparticle-based aerogels under visible light, significantly expanding the application potential of these novel three-dimensional photocatalysts.

ASSOCIATED CONTENT

Supporting Information

The Supporting Information is available free of charge at <https://pubs.acs.org/doi/10.1021/acsami.1c12579>.

Overview of all the samples with their names; temperatures of NH₃ treatment and NH₃ and Pd concentrations; drawings of the aerogel reactor and gas-phase reactor system; calculation of AQE(%); SEM image of Pd-TiO₂; crystallite size, surface area, and pore volume of Pd-TiO₂, NPT 300, NPT 350, NPT 400, and NPT 450; photographs of NPT 300, NPT 350, NPT 400, and NPT 450; XPS N 1s spectrum of Pd-TiO₂; XPS Ti 2p spectra of NPT 300, NPT 350, NPT 400, and NPT 450; XPS Pd 3d spectra of Pd-TiO₂ and NPT 350; UV-Vis diffuse reflectance spectra of TiO₂ and N-TiO₂ and visible light-driven photocatalytic H₂ production rate of TiO₂, N-TiO₂, Pd-TiO₂, Ar-Pd-TiO₂ 350, and NPT 350; powder XRD patterns of Pd-TiO₂ and Ar-Pd-TiO₂ 350; visible light-driven photocatalytic H₂ production and nitrogen concentration of NPT 350-C1, NPT 350-C2, NPT 350-C3, and NPT 350-C4; XPS N 1s and Ti 2p spectra of NPT 350-5, NPT 350-10, NPT 350-15, and NPT 350-20 (PDF)

AUTHOR INFORMATION

Corresponding Author

Markus Niederberger – Laboratory for Multifunctional Materials, Department of Materials, ETH Zurich, Zürich 8093, Switzerland; orcid.org/0000-0001-6058-1183; Email: markus.niederberger@mat.ethz.ch

Authors

Junggou Kwon – Laboratory for Multifunctional Materials, Department of Materials, ETH Zurich, Zürich 8093, Switzerland

Kyoungjun Choi – Nanoscience for Energy Technology and Sustainability, Department of Mechanical and Process Engineering, ETH Zurich, Zürich 8092, Switzerland

Murielle Schreck – Laboratory for Multifunctional Materials, Department of Materials, ETH Zurich, Zürich 8093, Switzerland

Tian Liu – Laboratory for Multifunctional Materials, Department of Materials, ETH Zurich, Zürich 8093, Switzerland

Elena Tervoort – Laboratory for Multifunctional Materials, Department of Materials, ETH Zurich, Zürich 8093, Switzerland

Complete contact information is available at: <https://pubs.acs.org/doi/10.1021/acsami.1c12579>

Notes

The authors declare no competing financial interest.

ACKNOWLEDGMENTS

Financial support by the Swiss National Science Foundation (project 200020B_184842) and by ETH Zürich is gratefully acknowledged. We thank Mr. Giovanni Cossu for providing XPS training and technical support. We also thank Till Kyburz for designing and producing the aerogel reactor. We appreciate the support from the Binning and Rohrer Nanotechnology Center of ETH Zürich and IBM Zürich.

REFERENCES

- (1) Schneider, J.; Matsuoka, M.; Takeuchi, M.; Zhang, J.; Horiuchi, Y.; Anpo, M.; Bahnemann, D. W. Understanding TiO₂ Photocatalysis: Mechanisms and Materials. *Chem. Rev.* **2014**, *114*, 9919–9986.
- (2) Tachikawa, T.; Tojo, S.; Kawai, K.; Endo, M.; Fujitsuka, M.; Ohno, T.; Nishijima, K.; Miyamoto, Z.; Majima, T. Photocatalytic Oxidation Reactivity of Holes in the Sulfur- and Carbon-Doped TiO₂ Powders Studied by Time-Resolved Diffuse Reflectance Spectroscopy. *J. Phys. Chem. B* **2004**, *108*, 19299–19306.
- (3) Hoang, S.; Berglund, S. P.; Hahn, N. T.; Bard, A. J.; Mullins, C. B. Enhancing Visible Light Photo-oxidation of Water with TiO₂ Nanowire Arrays via Cotreatment with H₂ and NH₃: Synergistic Effects between Ti³⁺ and N. *J. Am. Chem. Soc.* **2012**, *134*, 3659–3662.
- (4) Yu, J.; Xiang, Q.; Zhou, M. Preparation, Characterization and Visible-light-driven Photocatalytic Activity of Fe-Doped Titania Nanorods and First-Principles Study for Electronic Structures. *Appl. Catal. B* **2009**, *90*, 595–602.
- (5) Peiró, A. M.; Colombo, C.; Doyle, G.; Nelson, J.; Mills, A.; Durrant, J. R. Photochemical Reduction of Oxygen Adsorbed to Nanocrystalline TiO₂ Films: A Transient Absorption and Oxygen Scavenging Study of Different TiO₂ Preparations. *J. Phys. Chem. B* **2006**, *110*, 23255–23263.
- (6) Schreck, M.; Niederberger, M. Photocatalytic Gas Phase Reactions. *Chem. Mater.* **2019**, *31*, 597–618.
- (7) Niederberger, M. Multiscale Nanoparticle Assembly: From Particulate Precise Manufacturing to Colloidal Processing. *Adv. Funct. Mater.* **2017**, *27*, 1703647.
- (8) Wan, W.; Zhang, R.; Ma, M.; Zhou, Y. Monolithic Aerogel Photocatalysts: a Review. *J. Mater. Chem. A* **2018**, *6*, 754–775.
- (9) Rechberger, F.; Niederberger, M. Translucent Nanoparticle-Based Aerogel Monoliths as 3-Dimensional Photocatalysts for the Selective Photoreduction of CO₂ to Methanol in a Continuous Flow Reactor. *Mater. Horiz.* **2017**, *4*, 1115–1121.
- (10) Luna, A. L.; Matter, F.; Schreck, M.; Wohlwend, J.; Tervoort, E.; Colbeau-Justin, C.; Niederberger, M. Monolithic Metal-Containing TiO₂ Aerogels Assembled from Crystalline Pre-formed Nanoparticles as Efficient Photocatalysts for H₂ Generation. *Appl. Catal. B* **2020**, *267*, 118660.
- (11) Umebayashi, T.; Yamaki, T.; Tanaka, S.; Asai, K. Visible Light-Induced Degradation of Methylene Blue on S-doped TiO₂. *Chem. Lett.* **2003**, *32*, 330–331.
- (12) Li, D.; Haneda, H.; Hishita, S.; Ohashi, N. Visible-Light-Driven N–F–Codoped TiO₂ Photocatalysts. I. Synthesis by Spray Pyrolysis and Surface Characterization. *Chem. Mater.* **2005**, *17*, 2588–2595.
- (13) Kumaravel, V.; Mathew, S.; Bartlett, J.; Pillai, S. C. Photocatalytic Hydrogen Production using Metal Doped TiO₂: A Review of Recent Advances. *Appl. Catal. B* **2019**, *244*, 1021–1064.
- (14) Inturi, S. N. R.; Boningari, T.; Suidan, M.; Smirniotti, P. G. Visible-Light-Induced Photodegradation of Gas Phase Acetonitrile using Aerosol-Made Transition Metal (V, Cr, Fe, Co, Mn, Mo, Ni, Cu, Y, Ce, and Zr) Doped TiO₂. *Appl. Catal. B* **2014**, *144*, 333–342.
- (15) Primc, D.; Zeng, G.; Leute, R.; Walter, M.; Mayrhofer, L.; Niederberger, M. Chemical Substitution - Alignment of the Surface Potentials for Efficient Charge Transport in Nanocrystalline TiO₂ Photocatalysts. *Chem. Mater.* **2016**, *28*, 4223–4230.
- (16) Asahi, R.; Morikawa, T.; Ohwaki, T.; Aoki, K.; Taga, Y. Visible-Light Photocatalysis in Nitrogen-Doped Titanium Oxides. *Science* **2001**, *293*, 269–271.
- (17) Obata, K.; Irie, H.; Hashimoto, K. Enhanced Photocatalytic Activities of Ta, N Co-Doped TiO₂ Thin Films under Visible Light. *Chem. Phys.* **2007**, *339*, 124–132.
- (18) Irie, H.; Watanabe, Y.; Hashimoto, K. Nitrogen-Concentration Dependence on Photocatalytic Activity of TiO_{2-x}N_x Powders. *J. Phys. Chem. B* **2003**, *107*, 5483–5486.
- (19) Wang, J.; Tafen, D. N.; Lewis, J. P.; Hong, Z.; Manivannan, A.; Zhi, M.; Li, M.; Wu, N. Origin of Photocatalytic Activity of Nitrogen-Doped TiO₂ Nanobelts. *J. Am. Chem. Soc.* **2009**, *131*, 12290–12297.
- (20) Le, P.; Hieu, L.; Lam, T.-N.; Hang, N.; Truong, N.; Tuyen, L.; Phong, P.; Leu, J. Enhanced Photocatalytic Performance of Nitrogen-Doped TiO₂ Nanotube Arrays Using a Simple Annealing Process. *Micromachines* **2018**, *9*, 618.
- (21) Li, H.; Hao, Y.; Lu, H.; Liang, L.; Wang, Y.; Qiu, J.; Shi, X.; Wang, Y.; Yao, J. A Systematic Study on Visible-Light N-doped TiO₂ Photocatalyst Obtained from Ethylenediamine by Sol–Gel Method. *Appl. Surf. Sci.* **2015**, *344*, 112–118.
- (22) Sakhivel, S.; Kisch, H. Photocatalytic and Photoelectrochemical Properties of Nitrogen-Doped Titanium Dioxide. *ChemPhysChem* **2003**, *4*, 487–490.
- (23) Geng, J.; Yang, D.; Zhu, J.; Chen, D.; Jiang, Z. Nitrogen-Doped TiO₂ Nanotubes with Enhanced Photocatalytic Activity Synthesized by a Facile Wet Chemistry Method. *Mater. Res. Bull.* **2009**, *44*, 146–150.
- (24) Liu, C.; Zhang, L.; Liu, R.; Gao, Z.; Yang, X.; Tu, Z.; Yang, F.; Ye, Z.; Cui, L.; Xu, C.; Li, Y. Hydrothermal Synthesis of N-doped TiO₂ Nanowires and N-Doped Graphene Heterostructures with Enhanced Photocatalytic Properties. *J. Alloys Compd.* **2016**, *656*, 24–32.
- (25) Popa, M.; Macovei, D.; Indrea, E.; Mercioniu, I.; Popescu, I. C.; Danciu, V. Synthesis and Structural Characteristics of Nitrogen Doped TiO₂ Aerogels. *Microporous Mesoporous Mater.* **2010**, *132*, 80–86.
- (26) Horikawa, T.; Katoh, M.; Tomida, T. Preparation and Characterization of Nitrogen-Doped Mesoporous Titania with High Specific Surface Area. *Microporous Mesoporous Mater.* **2008**, *110*, 397–404.
- (27) Fort, C. I.; Pap, Z.; Indrea, E.; Baia, L.; Danciu, V.; Popa, M. Pt/N–TiO₂ Aerogel Composites Used for Hydrogen Production via Photocatalysis Process. *Catal. Lett.* **2014**, *144*, 1955–1961.
- (28) Asahi, R.; Morikawa, T.; Irie, H.; Ohwaki, T. Nitrogen-Doped Titanium Dioxide as Visible-Light-Sensitive Photocatalyst: Designs, Developments, and Prospects. *Chem. Rev.* **2014**, *114*, 9824–9852.
- (29) Niederberger, M.; Bartl, M. H.; Stucky, G. D. Benzyl Alcohol and Titanium Tetrachloride A Versatile Reaction System for the Nonaqueous and Low-Temperature Preparation of Crystalline and Luminescent Titania Nanoparticles. *Chem. Mater.* **2002**, *14*, 4364–4370.
- (30) Staniuk, M.; Rechberger, F.; Tervoort, E.; Niederberger, M. Adapting the Concepts of Nonaqueous Sol–Gel Chemistry to Metals: Synthesis and Formation Mechanism of Palladium and Palladium–Copper Nanoparticles in Benzyl Alcohol. *J. Sol-Gel Sci. Technol.* **2020**, *95*, 573–586.
- (31) Serpone, N.; Emeline, A. V. Suggested Terms and Definitions in Photocatalysis and Radiocatalysis. *Int. J. Photoenergy* **2002**, *4*, 91.
- (32) Heiligtag, F. J.; Rossell, M. D.; Süess, M. J.; Niederberger, M. Template-Free Co-Assembly of Preformed Au and TiO₂ nanoparticles into Multicomponent 3D Aerogels. *J. Mater. Chem.* **2011**, *21*, 16893.
- (33) Polleux, J.; Pinna, N.; Antonietti, M.; Hess, C.; Wild, U.; Schlögl, R.; Niederberger, M. Ligand Functionality as a Versatile Tool to Control the Assembly Behavior of Preformed Titania Nanocrystals. *Chem. Eur. J.* **2005**, *11*, 3541–3551.
- (34) Rechberger, F.; Ilari, G.; Willa, C.; Tervoort, E.; Niederberger, M. Processing of Cr Doped SrTiO₃ Nanoparticles into High Surface Area Aerogels and Thin Films. *Mater. Chem. Front.* **2017**, *1*, 1662–1667.

- (35) Chen, Q.; Ozkan, A.; Chattopadhyay, B.; Baert, K.; Poleunis, C.; Tromont, A.; Snyders, R.; Delcorte, A.; Terryn, H.; Delplancke-Ogletree, M.-P.; Geerts, Y. H.; Reniers, F. N-Doped TiO₂ Photocatalyst Coatings Synthesized by a Cold Atmospheric Plasma. *Langmuir* **2019**, *35*, 7161–7168.
- (36) Li, J.; Liu, C.-H.; Li, X.; Wang, Z.-Q.; Shao, Y.-C.; Wang, S.-D.; Sun, X.-L.; Pong, W.-F.; Guo, J.-H.; Sham, T.-K. Unraveling the Origin of Visible Light Capture by Core–Shell TiO₂ Nanotubes. *Chem. Mater.* **2016**, *28*, 4467–4475.
- (37) Di Valentin, C.; Finazzi, E.; Pacchioni, G.; Selloni, A.; Livraghi, S.; Paganini, M. C.; Giamello, E. N-doped TiO₂: Theory and Experiment. *Chem. Phys.* **2007**, *339*, 44–56.
- (38) Shifu, C.; Xuqiang, L.; Yunzhang, L.; Gengyu, C. The Preparation of Nitrogen-Doped TiO_{2-x}N_x Photocatalyst Coated on Hollow Glass Microbeads. *Appl. Surf. Sci.* **2007**, *253*, 3077–3082.
- (39) Tang, Y.-C.; Huang, X.-H.; Yu, H.-Q.; Tang, L.-H. Nitrogen-Doped TiO₂ Photocatalyst Prepared by Mechanochemical Method: Doping Mechanisms and Visible Photoactivity of Pollutant Degradation. *Inter. J. Photoenergy* **2012**, *2012*, 1–10.
- (40) Chen, H.; Nambu, A.; Wen, Graciani, J.; Zhong; Hanson, J. C.; Fujita, E.; Rodriguez, J. A. Reaction of NH₃ with Titania: N-Doping of the Oxide and TiN Formation. *J. Phys. Chem. C* **2007**, *111*, 1366–1372.
- (41) Yu, A.; Wu, G.; Zhang, F.; Yang, Y.; Guan, N. Synthesis and Characterization of N-doped TiO₂ Nanowires with Visible Light Response. *Catal. Lett.* **2009**, *129*, 507.
- (42) Di Valentin, C.; Pacchioni, G.; Selloni, A.; Livraghi, S.; Giamello, E. Characterization of Paramagnetic Species in N-Doped TiO₂ Powders by EPR Spectroscopy and DFT Calculations. *J. Phys. Chem. B* **2005**, *109*, 11414–11419.
- (43) Irie, H.; Washizuka, S.; Watanabe, Y.; Kako, T.; Hashimoto, K. Photoinduced Hydrophilic and Electrochemical Properties of Nitrogen-Doped TiO₂ Films. *J. Electrochem. Soc.* **2005**, *152*, E351.
- (44) Jaiswal, R.; Patel, N.; Kothari, D. C.; Miotello, A. Improved Visible Light Photocatalytic Activity of TiO₂ Co-Doped with Vanadium and Nitrogen. *Appl. Catal. B* **2012**, *126*, 47–54.
- (45) Zhang, P.; Fujitsuka, M.; Majima, T. TiO₂ Mesocrystal with Nitrogen and Fluorine Codoping during Topochemical Transformation: Efficient Visible Light Induced Photocatalyst with the Codopants. *Appl. Catal. B* **2016**, *185*, 181–188.
- (46) Wang, Z.; Yang, C.; Lin, T.; Yin, H.; Chen, P.; Wan, D.; Xu, F.; Huang, F.; Lin, J.; Xie, X.; Jiang, M. H-Doped Black Titania with Very High Solar Absorption and Excellent Photocatalysis Enhanced by Localized Surface Plasmon Resonance. *Advan. Funct. Mater.* **2013**, *23*, 5444–5450.
- (47) Zhou, Y.; Liu, Y.; Liu, P.; Zhang, W.; Xing, M.; Zhang, J. A Facile Approach to Further Improve the Substitution of Nitrogen into Reduced TiO₂– with an Enhanced Photocatalytic Activity. *Appl. Catal. B* **2015**, *170-171*, 66–73.
- (48) Llansola-Portoles, M. J.; Bergkamp, J. J.; Finkelstein-Shapiro, D.; Sherman, B. D.; Kodis, G.; Dimitrijevic, N. M.; Gust, D.; Moore, T. A.; Moore, A. L. Controlling Surface Defects and Photophysics in TiO₂ Nanoparticles. *J. Phys. Chem. A* **2014**, *118*, 10631–10638.
- (49) Zhou, L.; Cai, M.; Zhang, X.; Cui, N.; Chen, G.; Zou, G.-Y. In-Situ Nitrogen-Doped Black TiO₂ with Enhanced Visible-Light-Driven Photocatalytic Inactivation of *Microcystis Aeruginosa* Cells: Synthesis, Performance and Mechanism. *Appl. Catal. B* **2020**, *272*, 119019.
- (50) Novell-Leruth, G.; Valcárcel, A.; Pérez-Ramírez, J.; Ricart, J. M. Ammonia Dehydrogenation over Platinum-Group Metal Surfaces. Structure, Stability, and Reactivity of Adsorbed NH_x Species. *J. Phys. Chem. C* **2007**, *111*, 860–868.
- (51) Maeda, M.; Watanabe, T. Visible Light Photocatalysis of Nitrogen-Doped Titanium Oxide Films Prepared by Plasma-Enhanced Chemical Vapor Deposition. *J. Electrochem. Soc.* **2006**, *153*, C186.
- (52) Fakhouri, H.; Pulpytel, J.; Smith, W.; Zolfaghari, A.; Mortaheb, H. R.; Meshkini, F.; Jafari, R.; Sutter, E.; Arefi-Khonsari, F. Control of the Visible and UV Light Water Splitting and Photocatalysis of Nitrogen Doped TiO₂ Thin Films Deposited by Reactive Magnetron Sputtering. *Appl. Catal. B* **2014**, *144*, 12–21.
- (53) Balachandran, U.; Eror, N. G. Raman Spectra of Titanium Dioxide. *J. Solid State Chem.* **1982**, *42*, 276–282.
- (54) Naldoni, A.; Allieta, M.; Santangelo, S.; Marelli, M.; Fabbri, F.; Cappelli, S.; Bianchi, C. L.; Psaro, R.; Dal Santo, V. Effect of Nature and Location of Defects on Bandgap Narrowing in Black TiO₂ Nanoparticles. *J. Am. Chem. Soc.* **2012**, *134*, 7600–7603.
- (55) Wang, C.; Hu, Q.; Huang, J.; Wu, L.; Deng, Z.; Liu, Z.; Liu, Y.; Cao, Y. Efficient Hydrogen Production by Photocatalytic Water Splitting using N-Doped TiO₂ Film. *Appl. Surf. Sci.* **2013**, *283*, 188–192.
- (56) Huang, B.-S.; Wey, M.-Y. Properties and H₂ Production Ability of Pt Photodeposited on the Anatase Phase Transition of Nitrogen-Doped Titanium Dioxide. *Int. J. Hydrogen Energy* **2011**, *36*, 9479–9486.
- (57) Naik, B.; Moon, S. Y.; Kim, S. H.; Park, J. Y. Enhanced Photocatalytic Generation of Hydrogen by Pt-Deposited Nitrogen-Doped TiO₂ Hierarchical Nanostructures. *Appl. Surf. Sci.* **2015**, *354*, 347–352.